Image processing

The periodic contribution from the Si lattice was filtered out of the images using a singular-value decomposition. The Sb atom positions were determined from the filtered images using Source Extractor software[27]. Source Extractor smoothed the input images with a 0.5-Å-wide gaussian, then identified collections of pixels with an area consistent with the point-spread function of the STEM (~1.6 Å wide, which is six pixels in image x and four pixels in image y) and 1.5 standard deviations (σ) per pixel above the local background as objects. The chance of a false atom detection from random noise is thus at the 9σ and 6σ levels, respectively. Consequently, the image statistics are not expected to be sensitive to precise threshold values. A 1.5σ threshold was chosen because it was the lowest value that did not produce false positives in the undoped region of Fig. 1. The detection error between 0 and 1 Sb atoms is 3%, which is largely due to remnant thickness variations.

Received 21 December 2001; accepted 28 March 2002.

1. Packan, P. A. Pushing the limits. *Science* **285,** 2079–2081 (1999).
2. Muller, E. W. Study of atomic structure of metal surfaces in the field ion microscope. *J. Appl. Phys.* **28,** 1–6 (1957).
3. Crewe, A. V., Wall, J. & Langmore, J. Visibility of single atoms. *Science* **168,** 1338–1340 (1970).
4. Nellist, P. D. & Pennycook, S. J. Direct imaging of the atomic configuration of ultradispersed catalysts. *Science* **274,** 413–415 (1996).
5. *International Technology Roadmap for Semiconductors, Update 2000* (International SEMATECH, Austin, Texas, 2000); see http://public.itrs.net/Files/2000UpdateFinal/2kUdFinal.htm.
6. Gossmann, H.-J., Rafferty, C. S. & Keys, P. Junctions for deep sub-100 nm MOS: How far will ion implantation take us? *Mater. Res. Soc. Symp.* **610,** B1.2.1–B1.2.10 (2000).
7. Williams, J. S. & Short, K. T. Metastable doping behavior in antimony-implanted (100) silicon. *J. Appl. Phys.* **53,** 8663–8667 (1982).
8. Citrin, P. H., Muller, D. A., Gossmann, H.-J., Vanfleet, R. & Northrup, P. A. Geometric frustration of 2D dopants in silicon: surpassing electrical saturation. *Phys. Rev. Lett.* **83,** 3234–3237 (1999).
9. Fair, R. B. & Weber, G. R. Effect of complex formation on diffusion of arsenic is silicon. *J. Appl. Phys.* **44,** 273–279 (1973).
10. Mathiot, D. & Pfister, J. C. Diffusion of arsenic in silicon: validity of the percolation model. *Appl. Phys. Lett.* **42,** 1043–1044 (1983).
11. Pandey, K. C., Erbil, A., Cargill, C. S., Boehme, R. F. & Vanderbilt, D. Annealing of heavily arsenic-doped silicon: electrical deactivation and a new defect complex. *Phys. Rev. Lett.* **61,** 1282–1285 (1988).
12. Lawther, D. W. *et al.* Vacancy generation resulting from electrical deactivation of arsenic. *Appl. Phys. Lett.* **67,** 3575–3577 (1995).
13. Ramamoorthy, M. & Pantelides, S. T. Complex dynamical phenomena in heavily arsenic doped silicon. *Phys. Rev. Lett.* **76,** 4853–4756 (1996).
14. Saarinen, K. *et al.* Identification of vacancy-impurity complexes in highly n-type Si. *Phys. Rev. Lett.* **82,** 1883–1886 (1999).
15. Chadi, D. J. *et al.* Fermi-level pinning defects in highly n-doped silicon. *Phys. Rev. Lett.* **79,** 4834–4837 (1997).
16. Gossmann, H.-J., Unterwald, F. C. & Luftman, H. S. Doping of Si thin films by low-temperature molecular beam epitaxy. *J. Appl. Phys.* **73,** 8237–8241 (1993).
17. Muller, D. A. & Grazul, J. Optimizing the environment for sub-0.2 nm scanning transmission electron microscopy. *J. Electron Microsc.* **50,** 219–226 (2001).
18. Kirkland, E. J. *Advanced Computing in Electron Microscopy* (Plenum, New York, 1998).
19. Howie, A. Image contrast and localized signal selection techniques. *J. Microsc.* **17,** 11–23 (1979).
20. Pennycook, S. J. & Narayan, J. Metastable doping behavior in antimony-implanted (100) silicon. *Appl. Phys. Lett.* **45,** 385–387 (1984).
21. Kirkland, E. J., Loane, R. F. & Silcox, J. Simulation of annular dark field STEM images using a modified multislice method. *Ultramicroscopy* **23,** 77–96 (1987).
22. Loane, R. F., Kirkland, E. J. & Silcox, J. Visibility of single heavy atoms on thin crystalline silicon in simulated annular dark field. *Acta Cryst. A* **44,** 912–927 (1988).
23. Hillyard, S. E. & Silcox, J. Thickness effects in ADF STEM zone-axis images. *Ultramicroscopy* **52,** 325–334 (1993).
24. Hillyard, S. E. & Silcox, J. Detector geometry, thermal diffuse scattering and strain effects in ADF STEM imaging. *Ultramicroscopy* **58,** 6–17 (1995).
25. Delby, N., Krivanek, O. L., Nellist, P. D., Batson, P. E. & Lupini, A. R. Progress in aberration-corrected scanning transmission electron microscopy. *J. Electron Microsc.* **50,** 177–185 (2001).
26. Klepeis, S. J., Benedict, J. P. & Anderson, R. M. in *Mater. Res. Soc. Proc.* (ed. Bravman, J. C.) 179–190 (Materials Research Society, Pittsburgh, 1988).
27. Bertin, E. & Arnouts, S. SExtractor: software for source extraction. *Astron. Astrophys. Suppl. Ser.* **117,** 393–404 (1996).

Supplementary Information accompanies the paper on *Nature*'s website (http://www.nature.com).

Acknowledgements

We thank P. Mithra for introducing us to singular value decomposition, E. Kirkland for sharing his STEM image simulation codes, and D. Wittman for help with the Source Extractor software.

Competing interests statement

The authors declare that they have no competing financial interests.

Correspondence and requests for materials should be addressed to D. A. M. (e-mail: davidm@bell-labs.com).

Molecular segregation observed in a concentrated alcohol–water solution

S. Dixit*, J. Crain*, W. C. K. Poon*, J. L. Finney† & A. K. Soper‡

** Department of Physics and Astronomy, The University of Edinburgh, Mayfield Road, Edinburgh EH9 3JZ, UK*
† Department of Physics and Astronomy, University College London, Gower Street, London WC1E 6BE, UK
‡ ISIS Facility, Rutherford Appleton Laboratory, Chilton, Didcot, Oxon OX11 OQX, UK

When a simple alcohol such as methanol or ethanol is mixed with water[1,2], the entropy of the system increases far less than expected for an ideal solution of randomly mixed molecules[3]. This well-known effect has been attributed to hydrophobic headgroups creating ice-like or clathrate-like structures in the surrounding water[4], although experimental support for this hypothesis is scarce[5–7]. In fact, an increasing amount of experimental and theoretical work suggests that the hydrophobic headgroups of alcohol molecules in aqueous solution cluster together[2,8–10]. However, a consistent description of the details of this self-association is lacking[11–13]. Here we use neutron diffraction with isotope substitution to probe the molecular-scale structure of a concentrated alcohol–water mixture (7:3 molar ratio). Our data indicate that most of the water molecules exist as small hydrogen-bonded strings and clusters in a 'fluid' of close-packed methyl groups, with water clusters bridging neighbouring methanol hydroxyl groups through hydrogen bonding. This behaviour suggests that the anomalous thermodynamics of water–alcohol systems arises from incomplete mixing at the molecular level and from retention of remnants of the three-dimensional hydrogen-bonded network structure of bulk water.

In spite of considerable research into the nature of alcohol–water mixtures at the molecular level (see, for example, ref. 2 and several experiments and computer simulations[5,14–18]), there still seems to be little physical insight into the causes of the anomalous thermodynamic properties of alcohol–water mixtures. To investigate these matters, we perform a detailed determination of the methyl–methyl, methyl–water and water–water correlations in a concentrated mixture of methanol in water (7 methanol molecules:3 water molecules), using neutron diffraction with hydrogen isotope labelling. The diffraction data are interpreted by empirical potential structure refinement (EPSR; see Methods). Typical EPSR fits to our diffraction data on the methanol–water mixture are shown in Fig. 1. From the EPSR molecular ensembles, we derive site–site radial distribution functions (RDFs), $g_{\alpha\beta}(r)$, which describe the relative density of one type of atom, β, as a function of distance, r, from another type, α. (In this experiment, the labels α and β can each take on one of six possible atom types. They are C for methanol carbon, O for methanol oxygen, M for methyl hydrogen, H for hydroxyl hydrogen, O_W for water oxygen, and H_W for water hydrogen.) By comparing RDFs derived from our data with RDFs derived from previous diffraction data on pure methanol[19] and pure water[20], we examine how the local ordering of the methanol molecules is modified by the addition of small amounts of water. Although many of the individual site–site RDFs are not determined separately in the diffraction experiment (for example the O_W–O_W distribution), the EPSR procedure ensures that all the estimated RDFs are consistent with all the diffraction data.

The correlations between methanol molecules, as given by the $g_{CC}(r)$, $g_{MM}(r)$ and $g_{OO}(r)$ RDFs, are shown in Fig. 2 for both pure methanol and the concentrated aqueous mixture. Two notable features emerge: when water is added, the near-neighbour distance of the CC and MM functions shift to a lower radius by about 2% for

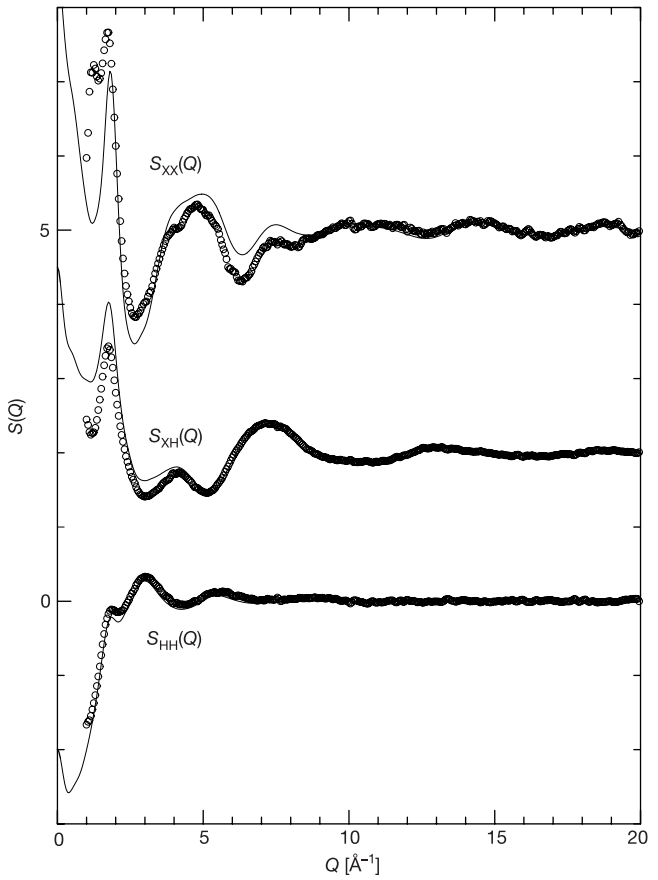

Figure 1 HH, XH and XX composite partial structure factors for a methanol–water mixture (70 mol% methanol). The case shown is where H/D substitution is performed on all hydrogen atoms (solutions (1), (6) and (7) in Methods). The measured structure factors are shown as the open circles. We note that the EPSR simulation fits simultaneously all nine composite structure factors, although only three of those fits (solid lines) are shown here. The lack of fit in some regions, particularly for the XX radial distribution function (RDF) at low wave vector transfer (*Q*), is believed to arise from residual nuclear recoil scattering (analogous to Compton scattering with X-rays) which is difficult to remove completely from the neutron data.

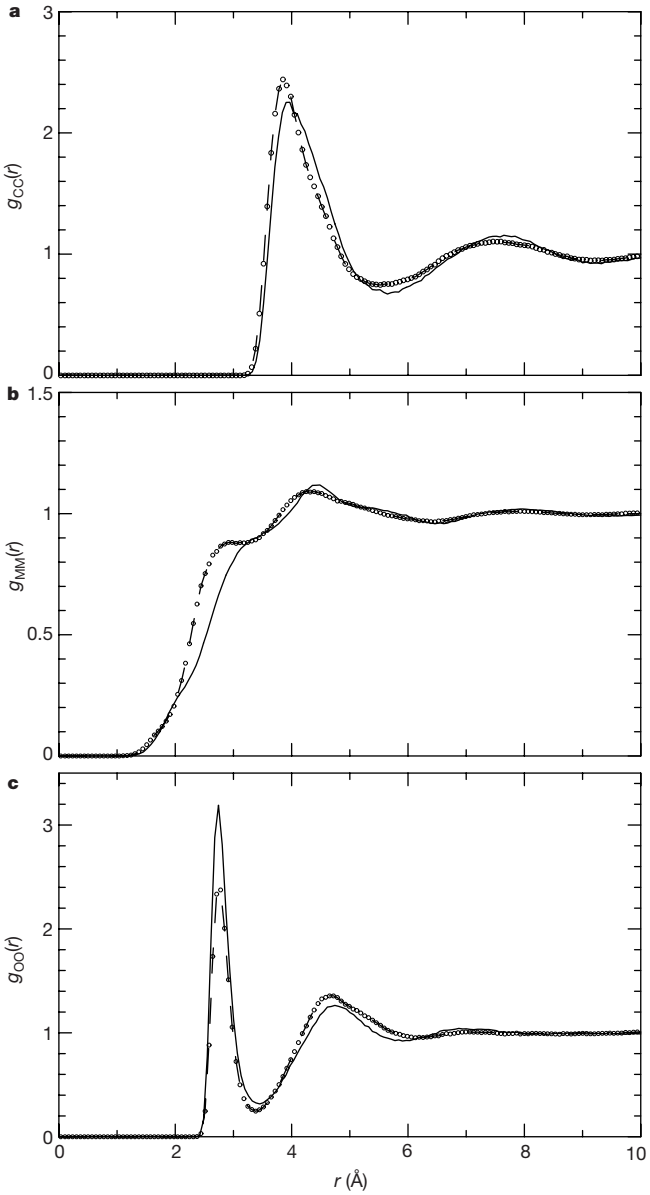

Figure 2 Methanol–methanol site–site radial distribution functions. **a**–**c**, The CC (**a**), MM (**b**), and OO (**c**) intermolecular methanol–methanol RDFs estimated from the structure refinement procedure for the methanol–water (7:3) mixture (dashed line, circles) are compared to the same functions for pure methanol (solid line). *r*, distance between atoms.

CC and more than this, by up to 20%, for MM. At the same time the first peak of the OO RDF does not move, but shrinks in size by about 50% and the second neighbour OO peak grows in amplitude and moves to a larger radius. The addition of water thus has the net effect of pressing the methyl headgroups closer together while pushing the methanol hydroxyl headgroups apart, which results in a reduction of the extent of methanol–methanol hydrogen bonding in the mixture.

The degree of hydrogen bonding in the two liquids before mixing is estimated by calculating coordination numbers for the OH and O_WH_W RDFs in pure methanol and pure water respectively. (We assume here that the OH coordination number up to the first minimum in the relevant OH RDF represents the number of hydrogen bonds associated with that atom pair.) This analysis indicates that there are ~1.8 hydrogen bonds per methanol molecule in pure methanol and ~3.6 hydrogen bonds per water molecule in pure water, yielding ~2.3 as the average number of hydrogen bonds per molecule for a system composed of 7 parts methanol and 3 parts water that have not yet been mixed. After mixing, hydrogen bonding will be manifested in several RDFs of water and methanol: OH, OH_W, HO_W RDFs for hydrogen bonds involving methanol molecules, and O_WH_W, O_WH, and H_WO RDFs for hydrogen bonds involving water molecules. In the 7:3 methanol–water mixture, we find ~1.2 methanol–methanol hydrogen bonds per methanol molecule but a further ~0.8 hydrogen bonds to water molecules, making the total number of hydrogen bonds per methanol molecule in the mixture ~2.0, that is, slightly higher than for pure methanol. For each water molecule present in the mixture, we find ~1.0 hydrogen bonds to other water molecules and 1.9 hydrogen bonds to methanol molecules, making the total number of hydrogen bonds per water molecule ~2.9, which is only 20% less than in pure water. For the mixture as a whole, the average number of hydrogen bonds per molecules is ~2.3 per molecule, that is, identical to the value for the same relative amounts of pure liquids before mixing. The hydrogen bonds between methanol and water molecules created upon mixing thus compensate almost exactly for the water–water and methanol–methanol hydrogen bonds lost upon mixing the pure liquids.

The water structure is analysed using the O_WO_W RDF, which is

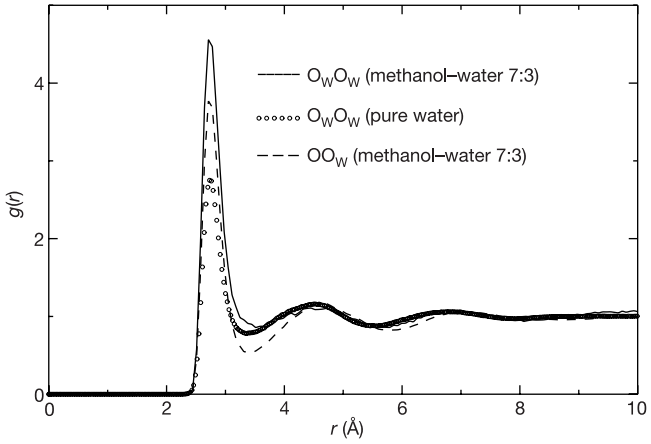

Figure 3 Water–water O_WO_W radial distribution functions. The methanol–water (7:3) O_WO_W RDF (solid line) is compared to the corresponding function for pure water (circles)[20], and with the methanol–water OO_W RDF in the methanol–water (7:3) mixture (dashed line).

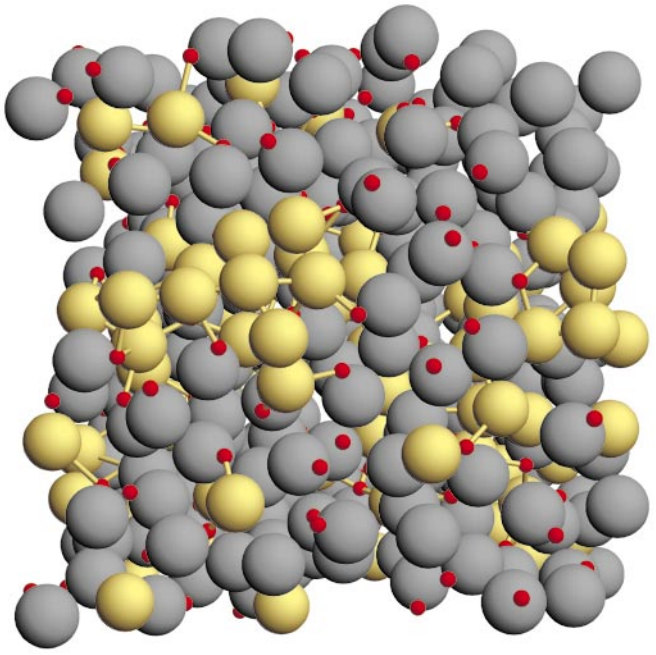

Figure 4 One of the simulated molecular boxes. Methyl groups are shown as grey spheres. Large yellow spheres have been used to highlight the positions of water molecules and small red spheres denote methanol oxygen atoms. This choice of sizes is to emphasize that the fact that the average methanol carbon to water oxygen distance is almost independent of the direction in which the water molecule is viewed from the methanol molecule (see ref. 5). Yellow bonds join water oxygen atoms to other oxygen atoms within their first coordination shell ($r < 3.5$ Å).

shown in Fig. 3 for both the mixture and pure water. The amplitude of the first peak of the O_WO_W RDF for the concentrated methanol solution is larger than that of the corresponding peak for pure water, but the shapes and positions are very similar. (We note however, that the O_WO_W near-neighbour coordination number, integrated out to 3.5 Å in both cases, drops from 5.0 ± 0.2 in pure water to 1.2 ± 0.2 in the methanol–water solution owing to the much lower water molecule number density in solution.) The second peak at about 4.5 Å, a signature of the hydrogen-bonded network present in pure water, is largely preserved in both position and amplitude in the concentrated alcohol mixture. Figure 3 also illustrates the correlation between water and the hydroxyl group of methanol, by showing the OO_W RDF. In this function, the second-neighbour peak near 4.5 Å is sharper than in the corresponding O_WO_W RDF of pure water, suggesting that the methanol hydroxyl group enhances tetrahedral structure in the water surrounding it. These results clearly contradict early predictions[1] that the water structure cannot exist in a concentrated alcohol–water solution.

A cluster analysis of the distribution of water molecules, derived from the simulation of the scattering data, provides further structural insight. If water and alcohol were randomly mixed at the molecular level, most water would exist as isolated molecules at the concentrations we have used, with distinct water clusters being rare. In practice although single water molecules (that is, cluster size 1) do occur, these constitute only about 13% of all the water molecules in the mixture. The remaining 87% water molecules occur in clusters or strings containing 2 to 20 or more molecules; the most likely structure is a three-water-molecule cluster. A snapshot of the simulation box (Fig. 4) shows groups of water molecules hydrogen-bonded together, forming small cavities in a 'fluid' of methyl headgroups. In this image, two water clusters can be seen left of centre and centre right, hydrogen-bonded to the hydroxyl groups of surrounding methanol molecules. The function of hydroxyl groups as bridges between methyl headgroups and water clusters explains why, on average, the methanol hydroxyl groups are further apart in the solution than in pure methanol. The concentration–temperature phase diagram of 0.7 molar aqueous methanol solution[21] shows that the system freezes only when cooled to approximately 170 K, suggesting that the water clusters we see can be supercooled to very low temperatures.

Frank and Evans[4] interpreted the observed excess entropies and enthalpies of solution for a wide range of solutes in terms of an 'iceberg' forming in the water surrounding a hydrophobic entity in aqueous solution. This appealing concept strongly influenced twentieth-century thinking about the way molecules interact in aqueous solution[11], although it was never confirmed by structural data. The present results challenge this interpretation: contrary to speculation that water structure is either enhanced or destroyed in an alcohol solution[1,2], we find that the local structure of water in a concentrated methanol–water solution is surprisingly close to its counterpart in pure water. Although we cannot calculate the entropy of mixing directly from our data, they do imply that the negative excess entropy observed in these systems[1,4] arises from incomplete mixing at the molecular level, rather than from water restructuring. We further suggest that the sign and magnitude of the excess enthalpy of mixing will be determined by an interplay between the relative strengths of the alcohol–alcohol, alcohol–water and water–water hydrogen bonds, because we find that the number of hydrogen bonds per molecule in solution is not significantly different from that in the pure liquids before mixing. The polar interaction of water with the alcohol hydroxyl group is thus likely to be a far more potent influence on the thermodynamic properties of alcohol–water mixtures than any water restructuring induced by the hydrophobic methyl groups. □

Methods

Diffraction experiment

Diffraction measurements were performed on the SANDALS diffractometer at ISIS. Seven isotopically substituted solutions (Aldrich Chemicals) were prepared: (1) CD_3OD in deuterated water, D_2O; (2) CH_3OD in D_2O; (3) A 50:50 mixture of solutions (1) and (2); (4) CD_3OH in H_2O; (5) a 50:50 mixture of solutions (1) and (4); (6) CH_3OH in H_2O; and (7) a 50:50 mixture of solutions (1) and (6). The solute–solute partial structure factor is obtained by isotope substitution on the methyl hydrogens using solutions (1), (2) and (3). Isotope substitution on the hydroxyl hydrogens of water and methanol as indicated in solutions (1), (4) and (5) gives correlations between all the hydroxyl hydrogens. Finally, solutions (1), (6) and (7) provide a measure of the correlations between all the hydrogens in the solutions, including the methanol–water correlations. Each of these three sets of solutions gives rise to three composite partial structure factors[22] $S_{HH}(Q)$, $S_{XH}(Q)$ and

$S_{XX}(Q)$, where H corresponds to the labelled hydrogen and X corresponds to the remaining unlabelled atoms for each set of three solutions.

Structure refinement

The nine composite partial structure factors which resulted from analysis of the diffraction data were used as constraints in an empirical potential structure refinement (EPSR)[23–25] simulation of the mixture, fixed at the experimental density and temperature. The cubic simulation box of side 26.77 Å contained 245 methanol and 105 water molecules. The seed potentials for the simulation were taken from the literature[15]. The EPSR procedure modifies these starting potential energy functions so as to make the simulated structure factors match as closely as possible the measured functions. An example of some of the fits is shown in Fig. 1. This leads to an ensemble of model molecular distributions that are consistent with the measured diffraction data.

Structure analysis

From these molecular assemblies, ensemble-averaged site–site radial distribution functions (RDFs), $g_{\alpha\beta}(r)$, can be estimated, as can other structural quantities as described below, all of which are consistent with the experimental data. Near-neighbour coordination numbers are estimated from these RDFs by integration: $N_{\alpha\beta} = 4\pi\rho_\beta \int_{r_{min}}^{r_{max}} g_{\alpha\beta}(r) r^2 \, dr$, where $N_{\alpha\beta}$ is the coordination number of β atoms around α atoms, ρ_β is the number density of β atoms in the liquid, and the range of integration is normally chosen to coincide with minima in the respective RDF. Uncertainties in these values are estimated from the observed fluctuations of $g_{\alpha\beta}(r)$ in the course of the simulation.

Cluster analysis is achieved by considering two water molecules to belong to the same cluster if they are separated by 3.5 Å or less—this is the position of the first minimum in the O_WO_W radial distribution function. The size of a water cluster is then determined by counting all the water molecules that lie within the specified distance range of each other.

Received 26 October 2001; accepted 4 March 2002.

1. Franks, F. & Ives, D. J. G. The structural properties of alcohol–water mixtures. *Q. Rev.* **20,** 1–45 (1966).
2. Franks, F. & Desnoyers, J. E. in *Water Science Reviews* Vol. 1 (ed. Franks, F.) 171–232 (Cambridge Univ. Press, 1985).
3. Murrell, J. N. & Jenkins, A. D. *Properties of Liquids and Solutions* 2nd edn 102–106 (Wiley, Chichester, 1994).
4. Frank, H. S. & Evans, M. W. Free volume and entropy in condensed systems. III. Entropy in binary liquid mixtures; partial molal entropy in dilute solutions; structure and thermodynamics in aqueous electrolytes. *J. Chem. Phys.* **13,** 507–532 (1945).
5. Soper, A. K. & Finney, J. L. Hydration of methanol in aqueous solution. *Phys. Rev. Lett.* **71,** 4346–4349 (1993).
6. Turner, J. & Soper, A. K. The effect of apolar solutes on water structure: alcohols and tetraalkylammonium ions. *J. Chem. Phys.* **101,** 6116–6125 (1994).
7. Bowron, D. T., Soper, A. K. & Finney, J. L. Temperature dependence of the structure of a 0.06 mole fraction tertiary butanol–water solution. *J. Chem. Phys.* **114,** 6203–6219 (2001).
8. Tsai, J., Gerstein, M. & Levitt, M. Keeping the shape but changing the charges: A simulation study of urea and its iso-steric analogs. *J. Chem. Phys.* **104,** 9417–9430 (1996).
9. Dixit, S., Poon, W. C. K. & Crain, J. Hydration of methanol in aqueous solutions: a Raman spectroscopic study. *J. Phys. Condens. Matter* **12,** L323–L328 (1999).
10. Wakisaka, A., Komatsu, S. & Usui, Y. Solute–solvent and solvent–solvent interactions evaluated through clusters isolated from solutions: preferential solvation in water–alcohol mixtures. *J. Mol. Liq.* **90,** 175–184 (2001).
11. D'Angelo, M., Onori, G. & Santucci, A. Self-association of monohydric alcohols in water: compressibility and infrared absorption measurements. *J. Chem. Phys.* **100,** 3107–3113 (1994).
12. Egashira, K. & Nishi, N. Low-frequency Raman spectroscopy of ethanol–water binary solution: evidence for self-association of solute and solvent molecules. *J. Phys. Chem. B* **102,** 4054–4057 (1998).
13. Yoshida, K. & Yamaguchi, T. Low temperature Raman spectroscopy of aqueous solutions of aliphatic alcohols. *Z. Naturforsch. A* **56,** 529–536 (2001).
14. Finney, J. L., Bowron, D. T. & Soper, A. K. The structure of aqueous solutions of tertiary butanol. *J. Phys. Condens. Matter* **12,** A123–A128 (2000).
15. Ferrario, M., Haughney, M., McDonald, I. R. & Klein, M. L. Molecular dynamics simulation of aqueous mixtures: methanol, acetone and ammonia. *J. Chem. Phys.* **93,** 5156–5166 (1990).
16. Palinkas, G., Hawlicka, E. & Heinzinger, K. Molecular-dynamics simulations of water–methanol mixtures. *Chem. Phys.* **158,** 65–76 (1991).
17. Tanaka, H. & Gubbins, K. Structure and thermodynamic properties of water–methanol mixtures. *J. Chem. Phys.* **97,** 2626–2634 (1992).
18. Laaksonen, A., Kusalik, P. G. & Svishchev, I. M. Three-dimensional structure in water–methanol mixtures. *J. Phys. Chem. A* **101,** 5910–5918 (1997).
19. Yamaguchi, T., Hidaka, K. & Soper, A. K. The structure of liquid methanol revisited: a neutron diffraction experiment at −80°C and +25°C. *Mol. Phys.* **96,** 1159–1168 (1999); Erratum **97,** 603–605 (1999).
20. Soper, A. K. The radial distribution functions of water and ice from 220 K to 673 K and at pressures up to 400 MPa. *Chem. Phys.* **258,** 121–137 (2000).
21. Murthy, S. S. N. Detailed study of ice clathrate relaxation: Evidence for the existence of clathrate structures in some water–alcohol mixtures. *J. Phys. Chem. A* **103,** 7927–7937 (1999).
22. Soper, A. K. & Luzar, A. A neutron diffraction study of dimethyl sulphoxide-water mixtures. *J. Chem. Phys.* **97,** 1320–1331 (1992).
23. Soper, A. K. Empirical potential Monte Carlo simulation of fluid structure. *Chem. Phys.* **202,** 295–306 (1996).
24. Bowron, D. T., Finney, J. L. & Soper, A. K. A structural investigation of solute–solute interactions in aqueous solutions of tertiary butanol. *J. Phys. Chem. B* **102,** 3551–3563 (1998).
25. Soper, A. K. Tests of the empirical potential structure refinement method and a new method of application to neutron diffraction data on water. *Mol. Phys.* **99,** 1503–1516 (2001).

Acknowledgements

S. D. is supported by the Edinburgh Chalmers Scholarship and the ORS award. Funding from the EPSRC Liquid Network and help from D. Bowron at an early stage of the experiments are gratefully acknowledged.

Competing interests statement

The authors declare that they have no competing financial interests.

Correspondence and requests for materials should be addressed to A.K.S. (e-mail: a.k.soper@rl.ac.uk).

Rapid freshening of the deep North Atlantic Ocean over the past four decades

Bob Dickson*, Igor Yashayaev†, Jens Meincke‡, Bill Turrell§, Stephen Dye* & Juergen Holfort‡

* *Centre for Environment, Fisheries, and Aquaculture Science, Lowestoft NR33 OHT, UK*
† *Bedford Institute of Oceanography, Dartmouth, Nova Scotia B2Y 4A2, Canada*
‡ *Institut fur Meereskunde, 22529 Hamburg, Germany*
§ *Marine Laboratory, PO Box 101, Aberdeen AB11 9DB, UK*

The overflow and descent of cold, dense water from the sills of the Denmark Strait and the Faroe–Shetland channel into the North Atlantic Ocean is the principal means of ventilating the deep oceans, and is therefore a key element of the global thermohaline circulation. Most computer simulations of the ocean system in a climate with increasing atmospheric greenhouse-gas concentrations predict a weakening thermohaline circulation in the North Atlantic as the subpolar seas become fresher and warmer[1–3], and it is assumed that this signal will be transferred to the deep ocean by the two overflows. From observations it has not been possible to detect whether the ocean's overturning circulation is changing, but recent evidence suggests that the transport over the sills may be slackening[4]. Here we show, through the analysis of long hydrographic records, that the system of overflow and entrainment that ventilates the deep Atlantic has steadily changed over the past four decades. We find that these changes have already led to sustained and widespread freshening of the deep ocean.

The Labrador Sea is a critical location for the Earth's climate system. In its upper and intermediate layers, annual-to-decadal variations in the production, character and thickness of its convectively formed mode water (Labrador Sea Water, LSW) directly determine the rate of the main Atlantic gyre circulation[5]. Through its deeper layers pass all of the deep and bottom waters that collectively form and drive the abyssal limb of the Atlantic meridional overturning circulation. Around its margins pass the two main freshwater flows from the Arctic Ocean to the North Atlantic (by way of the Canadian Arctic archipelago and the East Greenland shelf) that have been implicated in model experiments with a slowdown or shutdown of the meridional overturning circulation[1–3].

Over the past 3–4 decades, the entire water column of the Labrador Sea has undergone radical change. From 1966 to 1992, the overall cooling of the water column of the Labrador Sea was equivalent to a loss of $8\,W\,m^{-2}$ continuously for 26 years. Its freshening (Fig. 1a) was equivalent to mixing-in an extra 6 m of fresh water at the sea surface[6]. As a result, the steric height (caused by